RELATIVE ELEVATION DETERMINATION FROM LANDSAT IMAGERY

S. Wang, R.M. Haralick, J. Campbell

Dept. of Computer Science, Electrical Engineering, and Geography
Virginia Polytechnic Institute and State University

ABSTRACT

In LANDSAT imagery, spectral and spatial information can be used to estimate a relative digital terrain model in mountainous areas. To do this, the mixed information of direct and indirect illumination, material reflectance, and topographic modulation in the original LANDSAT imagery must be first separated. From the direct and indirect illumination information, ridges and valleys can be determined. From the material reflectance information, big visible rivers can be detected. Finally, a relative elevation model can be generated by elevation growing. In elevation growing valley pixels are assigned increasing elevations as they become more distant from the rivers or other valley pixels already assigned an elevation. It also proceeds in a direction perpendicular to valleys climbing up to the ridges assigning elevations to any unassigned pixel.

1. INTRODUCTION

It is a common task for a photointerpreter to examine the spatial pattern on an aerial image and by appropriate interpretation be able to tell the elevation of one area relative to another and be able to infer the stream network and the drainage network even though some of the streams may be below the resolution of the sensor. There is a wealth of information in spatial patterns on aerial imagery but most computer data processing of remotely sensed imagery, being limited to pixel spectral characteristics, does not make use of it.

In this paper, we describe a procedure by which the relative elevation model can be inferred from a LANDSAT scene of mountainous and hilly terrain. To a first order effect, the cause of the intensity value at any pixel is due to whether it is only diffusely lit or directly lit. If it is direcly illuminated there are additional effects due to the angle at which the sun illuminates the ground patch corresponding to the pixel and the reflectance of the surface material on the ground patch. To make sense of the spatial pattern first requires separation of these effects. For this purpose, we use a clustering technique on ratio images to determine similar reflectance classes and then do a subclustering on these classes to determine directly lit from indirectly lit pixels. This subclustering creates a shadow image. Then we modify the Eliason, Soderblom and Chavez [1981] technique to create two images from the one LANDSAT image (Haralick and Wang, 1983). The first image is a "reflectance" image; the second is a topographic modulation image portraging information related to surface slope and sun illumination. The details of this technique are given in Section 2.

As discussed in Section 3, the sun azimuth and the shadow image constitute sufficient information for the identification of the ridges and the valleys. With the valleys identified, each valley pixel may be assigned a relative elevation which increases as the valley path from the pixel to the river it empties in increases. Ridges must be assigned elevations higher than their neighboring valleys and each ridge pixel can be assigned a relative elevation which decreases on the ridge path from the pixel to the saddle point where the ridge crosses a valley. In order to do this, local slopes must be known. Some estimated local slopes are assigned initially to generate the first version of elevation model. Then the topographic modulation image is used to calculate more accurate local slopes to generate better elevation models. Finally, Landsat imagery is reconstructed to evaluate our illumination model and elevation reconstruction algorithm.

CH2014-9/84/0000/0150$01.00 © 1984 IEEE

1.1 Study Area

This research examines an area in southeastern West Virginia, shown in Figure 1.1. This region is a portion of the Appalachian Plateau's physiographic province, within the "unglaciated Allegheny plateau" described by Thornbury [1967]. In general, this region is a thoroughly dissected plateau-like surface. It receives about 1 meter of precipitation each year and, as depicted on topographic maps, has a moderate drainage network density. Drainage is through tributaries of the New (Kanawha) River, which flows west into the Ohio River drainage system.

The overall drainage pattern within this region is that of a relatively large sinuous channel (the Gauley River) superimposed over the finer texture of a dentritic pattern formed by first, second, and third order streams. A number of the small first or second order streams flow directly into the large channel. Thus the overall pattern is composed of a mixture of many very small stream segments, many with very steep gradients, a prominent major channel with a relatively low gradient, and relatively few stream segments of intermediate length and gradient.

Throughout the area, flood plains (when present) are narrow and tend to closely follow the course of the stream channel. Valleys are narrow, with steep sides; the Gauley River, for example, follows a valley that is typically 150 meters deep but only 100 meters wide. Uplands often consist only of ridge crests; although plateau-like upland regions are present, they are not continuous or extensive. The area is forested with a dense cover of deciduous trees (Kuchler's " mixed mesophytic forest") [1964]. Cleared areas for agriculture (chiefly pasture) tend to follow the valleys of intermediate-sized streams. Settlements are small and dispersed, usually positioned in valleys.

This region appears on the Charleston, West Virginia/Ohio USGS 1:250,000 quadrangle (NJ 17-5). Our investigations include areas in Nicholas County, W. VA and neighboring counties. This area was imaged by the LANDSAT-1 MSS on April 13, 1976 (scene id: 5360-14502; path 18, row 34). This date reflects important qualities of the scene. First, at this date the atmosphere was unusually clear--there is no evidence of atmospheric (Mie) scattering or degradation of the data. Also, at this spring date most of the forested areas are without leaves, especially at higher elevations. Lower elevations have a cover of newly-emerged leaves and grasses. Within a few weeks leaves will have emerged in vegetation throughout the entire region, but at this time in April, there is a sharp spectral contrast between the vegetation cover of the higher elevations and that of some of the valleys.

2. THE PROBLEM OF MIXED INFORMATION

Four kinds of information are mixed in LANDSAT imagery: surface reflectance, topography, diffuse light and haze. Assuming the ground surface is flat, vegetated areas have high reflectance for some spectral regions and appear as bright areas to the LANDSAT sensor. On the contrary, water areas have low reflectance and appear as dark areas to the LANDSAT sensor. If topography is then considered, there is a pattern of directly illuminated and shadowed slopes due to varied heights and orientations of the slopes. However, graytones for image pixels corresponding to shadowed locations are not zero because of diffuse light coming indirectly from the sun. Finally, when light is reflected from the ground back to the sensor, there is additive haze due to atmospheric scattering. The difficulty of interpreting LANDSAT scenes of mountainous areas is due to the mixing of topographic data with reflectance data. To begin to separate these individual components we need to begin with an illumination model.

2.1 Separating the Information

The basic data model for a Lambertian surface illuminated by a point source is

$$G(x,y) = r(x,y)\ I \cos\theta(x,y) \qquad (2.1)$$

where G is brightness value of a pixel within the image,
x,y are pixel coordinates,
r is surface reflectance,
I is the illumination flux from the sun, and
θ is the angle between sun incidence direction and surface normal (Figure 2.1).

Adding band number, diffuse light, and haze into this model, one has the general

model for LANDSAT data as:

I. For directly illuminated pixels

$$G(x,y,b) = r(x,y,b)\ I(b)\ \cos\theta(x,y) + r(x,y,b)\ D(b) + H(b)$$

II. For shadowed pixels

$$G(x,y,b) = r(x,y,b)\ D(b) + H(b) \qquad (2.2)$$

where b is the spectral band number,
D is diffuse light, and
H is the haze due to atmospheric scattering.

Because haze is an additive constant independent of pixel locations, we use the Switzer, Kowalik, and Lyon [1981] technique for haze removal. The haze corrected image G - H is defined as G'.

After haze is removed, it can be seen that resolution of the remaining components amounts to extracting diffuse light Df containing the information of r(x,y,b)D(b), reflectance data R which contains the information of r(x,y,b)I(b), and topographic modulation data Tp which contains the information of cosθ(x,y),

I. For directly illuminated pixels

$$G'(x,y,b) = R(x,y,b)\ Tp(x,y) + Df(x,y,b)$$

II. For shadowed pixels

$$G'(x,y,b) = Df(x,y,b) \qquad (2.3)$$

The first problem to be solved to accomplish this unmixing is the determination of which pixels are directly lit from which pixels are in shadow. Once this is accomplished the unraveling can begin. For example, for the diffuse light image, pixels which are in shadow take their value as the dehazed data value. Pixels which are direcly lit take their value as the average dehazed data value taken over all shadowed pixels which are likely to be from the same material as they are.

To separate the shadow pixels from the directly lit pixels, we seek to transform the images in a way in which the only effect is reflectance. Then within groups of pixels with similar reflectance, we can separate the bright appearing ones from the dark appearing ones. This two step technique is more accurate than a simple thresholding technique. (Campbell et. al, 1981, Wang et. al, 1983)

One way to transform the data so that the only remaining effect is reflectance is to take ratios of one band to another. The ratio image has been widely used by remote sensing researchers to subdue surface topographic effects [Vincent, 1973; Raines, et al, 1978]. An alternative ratioing procedure is to calculate a ratio of each pixel value in band to the total brightness for that pixel, summed over all bands, as suggested by Mulder (1982). For our procedure either approach is computationally feasible, provided the denominator in the ratio is composed of a linear combination of values. For this study, we prefer to use the ratios of individual pairs of bands, as ratios of band pairs are known to be effective in distinguishing reflectance of surface materials. (Eliason et. al, 1981). From Equation 2.2, the ratio image of two bands with band number b1 and b2 for directly illuminated pixels after haze is removed is

$$\frac{G'(x,y,b1)}{G'(x,y,b2)} = \frac{r(x,y,b1)[I(b1)\cos\theta(x,y) + D(b1)]}{r(x,y,b2)[I(b2)\cos\theta(x,y) + D(b2)]}$$

If one assumes illumination and diffuse light in bands b1 and b2 are related by

$$I(b1) = a\ I(b2),$$
$$D(b1) = a\ D(b2), \text{ then}$$

$$\frac{G'(x,y,b1)}{G'(x,y,b2)} = \frac{r(x,y,b1)\ a\ [I(b2)\cos\theta(x,y) + D(b2)]}{r(x,y,b2)\ \ [I(b2)\cos\theta(x,y)\ + D(b2)]} = a\ \frac{r(x,y,b1)}{r(x,y,b2)} \qquad (2.4.1)$$

Similarly, the ratio image for shadowed pixels is

$$\frac{G'(x,y,b1)}{G'(x,y,b2)} = a\,\frac{r(x,y,b1)}{r(x,y,b2)} \qquad (2.4.2)$$

Thus, whether shadowed or directly illuminated, the ratio image is independent of cosθ. Three independent ratio images taken from the 4-band imagery in Figure 1.1 are shown in Figure 2.2. It can be clearly seen that the effects of shadows have been removed.

2.2 Clustering

Because the three ratio images depend upon material reflectance only, regions of the same material reflectance can be identified by grouping together pixels of similar spectral characteristics. Because we desire to conduct the analysis using a minimum of prior information, unsupervised classification is favored over the supervised approach, which would require detail knowledge of the number, identify, and characteristics of groups. Unsupervised classification permits identification of the natural structure of the image with a minimum of prior information.

In the noisy ratio images of Figure 2.2, there are three major clusters: water area, vegetated area, and non-vegetated area. The size of water area is much smaller than that of the other two. For this reason, the mode approach [Goldberg and Shlien, 1978] which uses a fixed threshold to get cluster centers does not work. AMOEBA [Bryant, 1979] works better, but fails to obtain unbroken river segments. Despite its simplicity, it was found that ISODATA modified in such a way that class sizes are also taken into consideration works best.

Each material cluster cl can be defined as a set of pixels (x,y) in which Mc(x,y) = cl.

$$C(cl) = \{(x,y) \mid Mc(x,y) = cl\}$$

Once the material clusters are defined on the basis of the ratio images, one can find directly illuminated and shadowed pixels and define a binary shadow image. To do this, we collect together all dehazed 4-band pixel values belonging to a single material cluster and subcluster these 4-tuples into dark and bright subcluster classes. The next few paragraphs describe this in detail.

If one overlays the material cluster image Mc over any band of the dehazed image, one can see, within each material cluster, some pixels are bright and the others are dark. These differences are due to topographic variations; the bright pixels are directly illuminated pixels, and the dark pixels are in shadow. To separate the shadow pixels from the directly lit pixel, for each material cluster cl, one performs a subclustering on the dehazed pixel values in the set

$$\{G'(x,y,b) \mid Mc(x,y) = cl\}$$

which is the set of all dehazed values for pixels whose material cluster index is cl. This subclustering on cluster cl separates the directly illuminated pixels C0(cl) from the indirectly illuminated pixels Cl(cl):

$$C0(cl) = \{(x,y) \mid (x,y) \text{ is directly illuminated on the basis of the subclustering}\}$$

$$Cl(cl) = \{(x,y) \mid (x,y) \text{ is indirectly illuminated on the basis of the subclustering}\}$$

The subclustering of getting C0, Cl uses only the basic ISODATA program. In this case, the initial class mean for Cl includes all the minimum graytones for four bands, and the initial mean for C0 includes all the maximum graytones for four bands.

A shadow image Sw can be defined as

$$Sw : X \times Y \rightarrow \{0, 1\},$$

$$Sw : (x,y) = \begin{cases} 0 & \text{if } (x,y) \in C0(Mc(x,y)) \\ 1 & \text{if } (x,y) \in Cl(Mc(x,y)) \end{cases} \qquad (2.5)$$

The shadow image for Figure 1.1 is shown in Figure 2.3. The correspondence between this and topographic map is quite good. Now that directly lit and shadowed pixels have been identified, it is possible to use the dehazed image to get the diffuse light image Df, the reflectance image R, and the topographic modulation image Tp.

3. ELEVATION ESTIMATION

3.1 Identification of Ridges and Valleys

In the last section, the problem of confounded data is handled in such a way that the material information is contained in the reflectance image and the diffuse light image. The topographic information is contained in the shadow image and the topographic modulation image. In this section, we will show how to detect ridge segments, valley segments, and peak junctions from the shadow image. In the next section, we will perform an elevation growing to obtain initial raw estimates of elevations for all pixels on the basis of these ridge and valley segments. We then obtain a refined estimate by making the elevation model have slopes consistent with the information on the topographic modulation image.

Sides of hillsides facing the sun must be directly lit. Sides of hillsides facing away from the sun must be indirectly lit. A directly lit to indirectly lit transition in a direction moving away from the sun is a ridge. An indirectly lit to directly lit transition in a direction moving away from the sun is a valley. Thus, valleys and ridges exist on the borders between shadowed and directly lit areas. To find these areas we use the binary shadow image. First, a connected components operation determines regions on the shadow image. Then small, noisy regions are eliminated.

Next, the perimeters of these bright and shadowed regions are segmented into border segments according to their left regions, right regions, and orientations. A border segment is a maximally long sequence of connected pixels which are on the border between two given regions. Because the detection of ridges and valleys is highly orientation-dependent and the sun illumination comes from east in Figure 1.1, each border segment is further broken into several pieces according to orientation; all the east-west parts are separated from the north-south parts.

As the sun illumination is from the east in LANDSAT imagery, those border segments which are valley segments or ridge segments can be identified according to the brightness of the regions adjacent on the left and on the right. Because most of the trees in this area in April are unfoliated, the strongest region boundaries are shadow boundaries rather than reflectance boundaries, and the strongest boundaries are those at the extremes of steep slopes oriented normal to the sun direction. Because the sun illumination is predominantly east-west, a boundary that is dark on the left and bright on the right will correspond to a ridge, and the reverse will correspond to a valley.

East-west region boundaries are classified according to the labeling of neighboring north-south boundaries as well as their orientation relative to the east-west boundaries. As shown in Figure 3.1, each east-west boundary B1 has a left intersecting north-south boundary B2 and a right intersecting north-south boundary B3. If the angle between B1 and B2 is smaller than the angle between B1 to B3, then we assign the labeling of boundary B2 to B1; otherwise, we assign the labeling of boundary B3 to B1. The results of ridge-valley finding are shown in Figure 3.2.

3.2 Elevation Growing

The detection of the ridge and valley segments as discussed in the last section only assigns a ridge or valley label to them and does not assign relative elevations to them. This section describes how to estimate their relative elevations. First, a model called elevation growing is used to assign initial estimated elevations for all ridge and valley pixels. Next, interpolation is used to assign elevations for non-ridge and non-valley pixels.

The cross-sections of valleys are V-shaped, and the cross-sections of ridges are A-shaped. If one looks at topographic maps, the elevation contours of valleys such as those shown in Figure 3.3 can be frequently found. Thus, if one draws a line ab perpendicular to the valley Va, the elevations are increasing from point o to point a , and also from point o to point b. If the end point of a valley segment of smaller order is encountered during the growing, it is deduced that this end point is the lower end of this smaller valley segment. However, if a ridge point is encountered during

the process, the increasing has to stop because the elevation starts to decrease. Based on this knowledge, an "elevation growing" model can be created.

These results are shown in Figure 3.4 .

4. CONCLUSION

Two problems are addressed in this paper: definition of an illumination model and computation of an elevation model. First, an illumination model was defined and a series of steps was used to extract the shadow image, the diffuse light imagery, the reflectance imagery, and the topographic modulation image. The success of the process depends largely on clustering.

Next, knowing the sun azimuths and shadow image the ridges and valleys were found. An elevation growing process from valleys to ridges was found to be efficient in reconstructing the elevation model. Then an iterative method improved the elevation model by making it as consistent as possible with the topographic modulation image.

The techniques of this research work best for areas having big shadow areas. If water areas cannot be found to help identify the lowest valley locations, the elevation understanding problem will be more complicated. Other applications of this technique include the refinement of a given coarse digital elevation model using higher resolution multispectral imagery. In this kind of application, the given digital elevation model essentially calibrates the elevation growing process so that the resulting refinement constitutes a smart interpolation process.

REFERENCES

[1] T.T. Alfoldi and J.C. Munday, Jr., Water Quality Analysis by Digital Chromaticity Mapping of LANDSAT Data, Canadian J. of Remote Sensing, 4 (2): 108 - 126, 1978.

[2] J. Bryant, On the Clustering of Multidimensional Pictorial Data, Pattern Recognition, Vol. II, pp. 115-125, 1979.

[3] J. Campbell, R. W. Ehrich, D. Elliott, R. M. Haralick, S. Wang, Spatial Reasoning in Remotely Sensed Data, Proceedings for the 15th International Symposium on Remote Sensing of Environment, May 11 - 15, 1981, Ann Arbor, Michigan.

[4] R.O. Duda and P.E. Hart, Pattern Classification and Scene Analysis, Wiley, 1973.

[5] P.T. Eliason, L.A. Soderblom, and P.S. Chavez, Jr., Extraction of Topographic and Spectral Albedo Information from Multispectral Images, Photogrammetric Engineering and Remote Sensing, Vol. 48, No. 11, Nov. 1981, pp. 1571-1579.

[6] M. Goldberg and S. Shlien, A Clustering Scheme for Multispectral Images, IEEE Transactions on Systems, Man, and Cybernetics, Vol. 8, No. 2, 1978.

[7] R. M. Haralick, S. Wang, Relative Elevation Determination From Landsat Imagery, Proceedings, COMPCON, September, 1983, Washington, D.C.

[8] R.M. Haralick, S. Wang, D.B. Elliott, Spatial Reasoning to Determine Stream Network from Landsat Imagery, 6th International Conference on Pattern Recognition, 1982, Munich, Germany.

[9] A.W. Kuchler, Potential Natural Vegetation of the Conterminous United States, American Geographical Society Special Publication, No. 36, 1964.

[10] J. G. Moik, Digital Processing of Remotely Sensed Images, NASA sp - 431, 1980.

[11] N.C. Mulder Methology of Color Coding MSS and Other Data. Paper presented at Inter-Congress Symmposium, Commission III (Mathematicla Models, Accuray Aspects, and Quality Control), International Society of Photogrammetry and Remote Sensing, 1982, Otaniemi, Finland.

[12] National Cartographic Information Center, Digital Terrain Tapes, User Guide, Second Edition, 1980.

[13] G.L. Raines, T.W. Offield, and E.S. Santos, Remote Sensing and Subsurface Definition of Faceies and Structure Related to Uranium Deposits, Powder River Basin, Wyomihg, Econ. Geol., V73, pp.1706-1723, 1978.

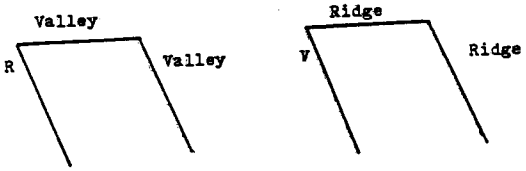

Figure 3.1 - Classifying east-west border segments

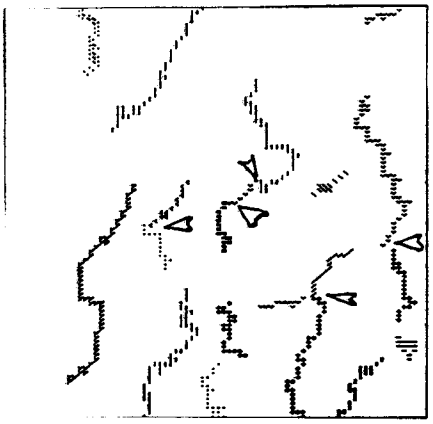

Figure 3.2b Ridge map consisting of the border segments which are identified as ridges

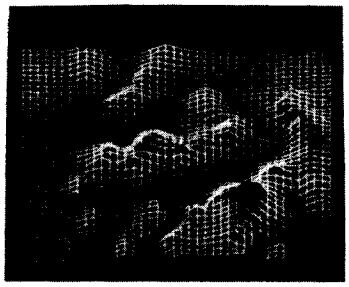

Figure 3.4a- Elevation model by using Laplacian mask.

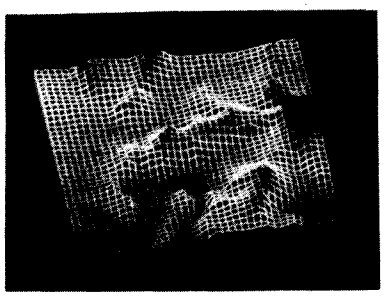

Figure 3.4b - Optimal elevation image.

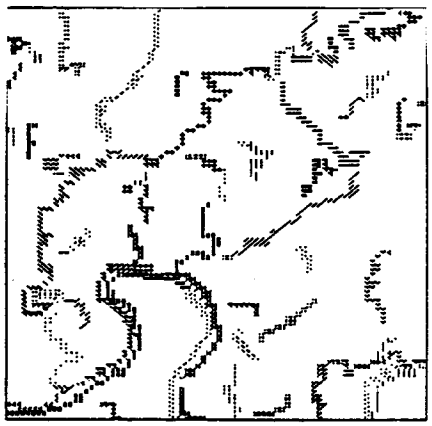

Figure 3.2a Valley map consisting of the border segments which are identified as valleys.

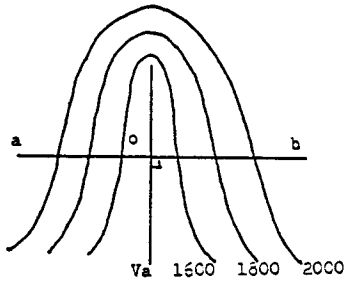

Figure 3.3 - The elevation of valleys and its relation to elevation growing

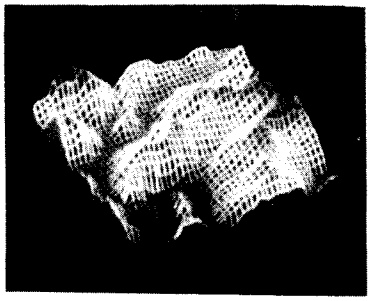

Figure 3.4c- Elevation data from digital terrain tape.